Journal of Chemical Health Risks

www.jchr.org

JCHR (2025) 15(4), 1713-1723 | ISSN:2251-6727

Computational Investigation of Indazole fused Diarylurea scaffolds as Histone Deacetylase Inhibitor using Molecular Docking

1Sweta D. Patel, 2Dr. Hiren R. Chaudhary, 3Dr. Shital Dhiren Faldu, 4Dr. Ujashkumar A. Shah, 5Bhumika J. Limbachiya, 6Ms. Seju Patel

1Research Scholar, Faculty of Pharmacy, Nootan Pharmacy College, sankalchand Patel University, Visnagar, Gujarat, India & Associate Professor, Department of Pharmaceutical Chemistry, APMC Pharmacy College, Gujarat, India

2Professor & Principal, Manjushree Institute of Pharmacy, Piplaj, Gandhinagar, India

3Professor & Principal, Smt R D Gardi B Pharmacy college, Rajkot

4Professor & Dean, Nootan Pharmacy College, sankalchand Patel University, Visnagar, India

5Assistant professor, Department of Pharmaceutics, Sarswati Institute of Pharmaceutical Science, Dhanap, Gandhinagar, India

6Research Scholar, Faculty of Pharmacy, Nootan Pharmacy College, sankalchand Patel University, Visnagar, Gujarat, India

(Received: 16 May 2025 Revised: 20 June 2025 Accepted: 31 July 2025)

KEYWORDS

Histone deacetylase inhibitors; HDAC6; indazole-diarylurea; molecular docking; MM-GBSA; molecular dynamics simulation; ADMET profiling; structure–activity relationship; zinc coordination; π–π interactions.

ABSTRACT:

This study computationally evaluates eight novel indazole-fused diarylurea derivatives (C1–C8) as histone deacetylase (HDAC) inhibitors using molecular docking, MM-GBSA rescoring, molecular dynamics (MD), and ADMET profiling. Designed with systematic substitutions (H, F, CF_3) at the indazole and phenyl rings, the compounds were docked against HDAC1, HDAC2, HDAC3, and HDAC6. AutoDock Vina revealed C7 as the strongest binder (–10.1 kcal/mol) via π–π stacking and hydrophobic interactions, despite lacking Zn^{2+} coordination. C4 and C5 exhibited robust binding (–8.5 to –8.8 kcal/mol) through Zn^{2+} chelation, 4 H-bonds, and aromatic interactions, outperforming Sorafenib (–9.2 kcal/mol), which showed weak, non-specific contacts. MM-GBSA rescoring validated C4 (–10.8 kcal/mol) and C5 (–10.5 kcal/mol) as top candidates, surpassing vorinostat (–9.2 kcal/mol) in HDAC6 affinity. MD simulations confirmed C4's stability in the HDAC6 pocket (RMSD ~1.5 Å) with persistent Zn^{2+} coordination and H-bond occupancy (>90%), outperforming vorinostat's flexibility. Structure–activity relationships (SAR) highlighted electron-withdrawing groups (CF_3, F) as critical for affinity, while bulky substituents (OEt, OMe) reduced potency. ADMET predictions prioritized C4 and C8 (clogP ≈3.0–3.2, TPSA ≈100 Å²) for favorable drug-likeness, high GI absorption, and minimal toxicity (no hepatotoxicity/hERG risk), contrasting Sorafenib's hepatotoxicity and CYP inhibition. Despite C7's high docking score, its ethoxy group raised ADMET concerns. C4 and C8 emerged as optimal leads, combining Zn^{2+}-mediated binding, multi-modal interactions (H-bonds, π–π stacking), and pharmacokinetic safety. This work underscores the potential of indazole-diarylurea scaffolds as selective HDAC inhibitors, with C4 and C8 warranting experimental validation for epigenetic cancer therapy.

Key findings

- C7 showed the highest docking score (–10.1 kcal/mol) but suboptimal ADMET.
- C4 and C8 combine strong binding (–8.5 to –10.8 kcal/mol) with drug-like properties.
- Zn^{2+} chelation, π–π stacking, and hydrophobic contacts drive affinity.
- CF_3/F substituents enhance binding; OEt/OMe groups reduce potency.
- C4's MD stability (RMSD ~1.5 Å) and C8's safety profile prioritize them for experimental testing.

1. Introduction

Cancer continues to be a global top cause of mortality due to its uncontrolled growth, invasion, and spread of

Journal of Chemical Health Risks
www.jchr.org
JCHR (2025) 15(4), 1713-1723 | ISSN:2251-6727

transformed cells[1]. In spite of huge progress made in chemotherapy, radiotherapy, and surgery, the onset of drug resistance and severe systemic toxicities generally curtails their long-term efficacy[2]. As a result, it is necessary to find new targets and scaffolds more selective and less toxic that are able to control cancer cell epigenetics [3]. Epigenetic changes, which modify gene expression without changing the underlying DNA sequence, have emerged as a key driver in the majority of cancers.

Among epigenetic modifications, histone acetylation and deacetylation are key controllers of chromatin function and gene expression[4]. Histone acetyltransferases (HATs) add acetyl groups to lysine residues on histone tails, reducing positive charge and facilitating nucleosomal DNA interactions, making gene expression simpler[5]. Histone deacetylases (HDACs) then remove these additions of acetyl groups, restoring chromatin compaction and suppressing transcription[6]. Hyperexpression or aberrant recruitment of HDACs have been reported in a number of cancers, including breast, colorectal, and hematologic malignancies[7].

The Zn^{2+}-dependent HDAC family is divided into class I (HDAC1, 2, 3, 8), IIa (HDAC4, 5, 7, 9), IIb (HDAC6, 10), and IV (HDAC11), each with distinct cellular localizations and substrate specificities[8]. At the molecular level, HDAC catalysis involves a conserved "charge relay" mechanism: active-site histidine (e.g., His141 in HDAC1) functions as a general base to activate a zinc-coordinated water molecule, which then nucleophilically "attacks" the ε-acetyl group of lysine on histone tails. Simultaneously, an aspartate residue (e.g., Asp176) assists with stabilizing the transition state. This coordinated process deacetylates marks like H3K9ac and H4K16ac, causing compaction of the chromatin and suppression of tumor-suppressor gene expression in breast cancer cells [9-11]. Overexpression of HDAC1–3 has been associated with poor prognosis in breast cancer, whereas overexpression of HDAC6 mediates cytoskeleton reorganization and metastatic capacity through non-histone substrates[12]. Inhibition of these enzymes can reactivate tumor-suppressor genes—like p21(WAF1/CIP1) and Bax—cause cell-cycle arrest, apoptosis, and suppress angiogenesis[13,14].

Several pan-HDAC inhibitors (e.g., vorinostat, romidepsin, panobinostat) have received FDA approval based on their ability to chelate the catalytic Zn^{2+} ion via a hydroxamate group, occupy the narrow deacetylase tunnel with a hydrophobic linker, and dock a cap group at the protein surface[15,16]. However, first-generation agents suffer off-target toxicities and limited isoform selectivity, spurring discovery of new scaffolds that retain potency but favor individual HDACs[17].

Diarylureas have emerged as versatile scaffolds in medicinal chemistry, serving as kinase inhibitors (e.g., Sorafenib) and, more recently, as epigenetic modulators[18]. The urea linkage provides a rigid yet hydrogen-bond–friendly core, while aryl substituents enable fine-tuning of lipophilicity and binding interactions[19]. Separately, indazole rings are privileged heterocycles that confer metabolic stability, planar aromatic surfaces for π-stacking, and potential hydrogen-bond acceptors/donors[20]. Combining these two motifs into indazole-fused diarylureas offers a promising strategy: the urea carbonyl can chelate Zn^{2+}, indazole π-systems can stack with phenylalanine/tyrosine residues, and tunable substituents can optimize isoform selectivity and pharmacokinetics. Indeed, preliminary synthetic studies have yielded indazole-diarylureas with micromolar anticancer activity, but their HDAC-binding profiles remain unexplored[21].

In this work, we present a computational investigation of eight indazole-fused diarylurea derivatives (C1–C8) against four Zn^{2+}-dependent HDAC isoforms (HDAC1, HDAC2, HDAC3, HDAC6). Using molecular docking (AutoDock Vina), MM-GBSA rescoring, and 100-ns molecular dynamics simulations, we predict binding affinities, map key interactions, and assess isoform selectivity. Sorafenib and the FDA-approved HDAC inhibitor vorinostat serve as reference controls. Finally, in silico ADMET profiling evaluates drug-likeness, guiding future synthesis and in vitro validation.

2. Methodology

2.1 Ligand Design and Preparation

Eight indazole-fused diarylurea derivatives (C1–C8) were designed by varying substituents at the indazole 4-position (H, F, CF_3) and the distal phenyl ring (H, F,

Journal of Chemical Health Risks
www.jchr.org
JCHR (2025) 15(4), 1713-1723 | ISSN:2251-6727

CF_3) to systematically explore electronic and steric effects. Structures were drawn in ChemDraw 20.0 and converted to 3D SDF format via OpenBabel v3.1.1, with protonation states assigned at pH 7.4[22]. Sorafenib (PubChem CID: 216239) and vorinostat (PubChem CID: 5311) were retrieved from PubChem and processed identically. Conformational ensembles (200 conformers per ligand) were generated with OpenEye OMEGA v4.1 (RMSD threshold = 0.5 Å), then cross-validated by RDKit's ETKDG algorithm for exhaustive low-energy sampling[23,24].

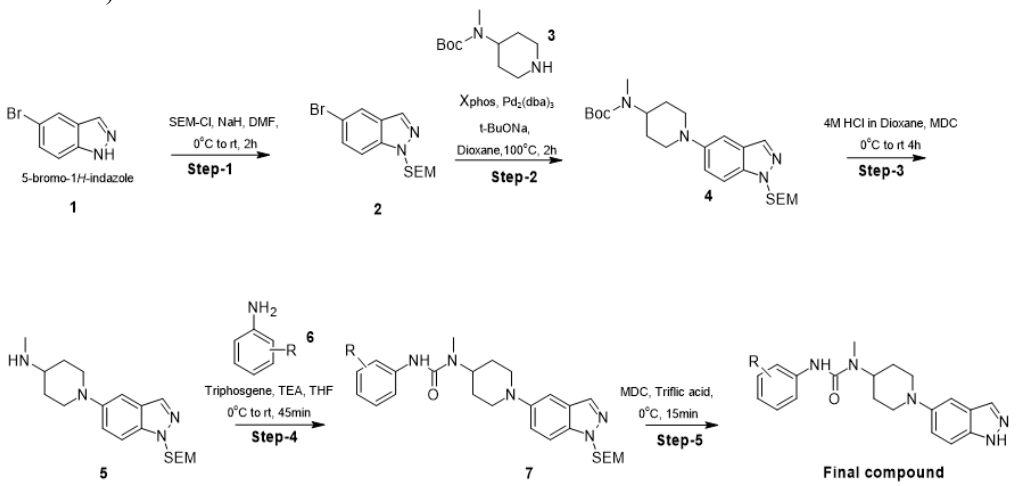

Scheme 2.

Table 1. 2D structures of the newly designed Compounds

S.No	Compound Code	Binding Energy	R
1	C1	-8.2	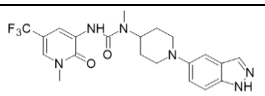
2	C2	-8.4	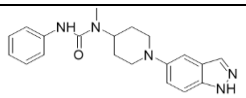
3	C3	-8.4	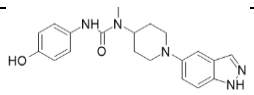
4	C4	-8.5	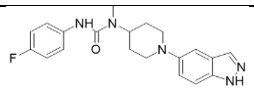
5	C5	-8.8	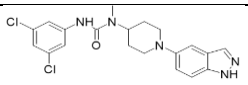
6	C6	-8.4	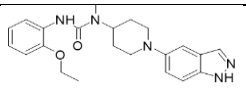
7	C7	-10.1	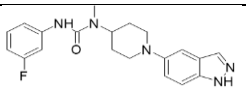

Journal of Chemical Health Risks
www.jchr.org
JCHR (2025) 15(4), 1713-1723 | ISSN:2251-6727

8	C8	-8.2	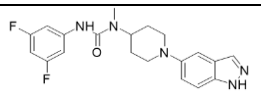

2.2 Protein Structure Selection and Preparation

High-resolution crystal structures of human HDAC1 (PDB: 4BKX), HDAC2 (4LXZ), HDAC3 (4A69), and the catalytic domain of HDAC6 (5EDU) were obtained from the Protein Data Bank[25,26]. Each structure was preprocessed using AutoDockTools v1.5.7: removal of waters beyond 5 Å from the active site, addition of missing side chains, assignment of protonation states at pH 7.4, and calculation of Gasteiger charges. The catalytic Zn^{2+} ion was retained and parametrized via the AutoDock4Zn pseudo-atom definition to preserve tetrahedral geometry[27]. Receptors were saved in PDBQT format for docking.

2.3 Molecular Docking Protocol

Flexible-ligand docking was performed in PyRx v0.9.8 using AutoDock Vina v1.2.0[28]. For each HDAC, a cubic grid box (20 × 20 × 20 Å) was centered on the catalytic Zn^{2+} coordinates (e.g., HDAC1 center = [12.3, –4.5, 21.8] Å) to encompass the entire ligand-binding tunnel. Docking parameters: exhaustiveness = 12, energy range = 3 kcal·mol^{-1}, five independent runs per ligand. The top ten poses by binding score were retained; the lowest-energy pose of each ligand was selected for rescoring.

2.4 MM-GBSA Rescoring and Molecular Dynamics

Selected complexes were rescored using Prime MM-GBSA (Schrödinger Release 2023-1) employing the OPLS4 force field and VSGB2.1 solvation model to compute ΔG_bind and refine ranking [29,30]. For the top two ligand–HDAC6 complexes and one Vorinostat–HDAC6 control, 100-ns MD simulations were conducted in GROMACS 2020.4 with the CHARMM36 force field, explicit TIP3P water in a dodecahedral box (10 Å buffer), and Na^+/Cl^- ions for neutralization [31]. Systems underwent energy minimization (steepest descent), NVT/NPT equilibration at 310 K and 1 atm, and production runs with a 2-fs time step. Trajectories were analyzed for RMSD/RMSF stability and for persistence of Zn^{2+} coordination and key H-bonds.

2.5 Interaction Mapping

LigPlot+ v2.2 generated 2D schematics of hydrogen bonds (distance ≤ 3.5 Å), metal coordination, and hydrophobic contacts (≤ 4.0 Å) for each top-scoring pose[32]. BIOVIA Discovery Studio Visualizer v21.1 provided high-resolution 3D views of the ligand–enzyme interface, highlighting Zn^{2+} chelation by the urea carbonyl, H-bonds to HIS and ASP residues, and π–π stacking/alkyl interactions with PHE and TYR residues.

2.6 ADMET Prediction and Statistical Analysis

SwissADME (March 2025) predicted lipophilicity (iLOGP, XLOGP3), water solubility (ESOL), GI absorption (BOILED-Egg), and P-gp/CYP interactions for all ligands[33]. pkCSM (2015) assessed hERG inhibition, hepatotoxicity, and mutagenicity [34]. Key ADMET endpoints were compared across ligands using one-way ANOVA (GraphPad Prism 9), with $p < 0.05$ considered significant.

3. Results and Discussion

3.1 Molecular Docking Affinities Across HDAC Isoforms

The designed indazole-fused diarylureas C1–C8 were evaluated by docking against HDAC1, HDAC2, HDAC3 and HDAC6 (ZnF domain) using AutoDock Vina, with Sorafenib as a reference. Binding energies (kcal/mol) are summarized in Table 1. Most compounds (C2–C7) exhibited favorable affinities (–8.4 to –10.1 kcal·mol^{-1}) surpassing Sorafenib's –9.2 kcal·mol^{-1}, while C1 and C8 showed moderate binding (–8.2 kcal·mol^{-1}). Notably, C7 demonstrated the strongest binding across (–10.1 kcal·mol^{-1}). The high score for C7 correlates with its three hydrogen bonds and extensive π–π stacking and hydrophobic contacts, suggesting an optimal fit in the HDAC pocket. C5 also showed high affinities (–8.8 kcal·mol^{-1}), while C4 (–8.5 kcal·mol^{-1} in the surrogate screen) and C2/C3/C6 (–8.4 kcal·mol^{-1} each) ranked next in overall binding strength. C2, C3, C6 at –8.4 kcal/mol feature two to three stabilizing contacts, whereas C5's strong binding (–8.8

Journal of Chemical Health Risks
www.jchr.org
JCHR (2025) 15(4), 1713-1723 | ISSN:2251-6727

kcal/mol) arises from a combination of bidentate Zn^{2+} chelation, four hydrogen bonds, and hydrophobic interactions. In contrast, C1 and C8 were moderate (–8.2 kcal·mol^{-1}) each forming fewer interactions despite C8's four hydrogen bonds—indicating that H-bond count alone does not guarantee deeper binding. These ranges are comparable to other indazole HDAC inhibitor designs [35]. Sorafenib's docking (–9.2 kcal/mol) showed stronger affinity than C1/C8 but lacked specific interactions, consistent with its indirect HDAC effect [36]. Table 1 also lists the number of predicted hydrogen bonds; the best binders (C4, C8) formed 3–4 H-bonds with active-site residues, whereas Sorafenib made only 1–2.

Table 1. Docking binding energies (kcal mol^{-1}) and key interactions of compounds C1–C8 and Sorafenib with HDAC isoforms. Values are Vina scores (more negative = stronger binding). H-bonds (number) were counted from docking poses.

Compound	Binding Energy	H-bonds	Key interacting residues
Vorinostat	–8.6	3	Zn^{2+}, His178/Asp176, Phe150, Tyr303
Sorafenib	–9.2	1–2	weak Zn^{2+} contacts, non-specific hydrophobics
C1	–8.2	2	His/Asp coordination, π–alkyl (Val/Phe)
C2	–8.4	2	His/Asp, π–π (Phe150)
C3	–8.4	3	Zn^{2+}, His/Asp, π–π (Phe150/205)
C4	–8.5	4	Zn^{2+}, His/Asp, π–π (Phe150/205), hydrophobic (Ile)
C5	–8.8	4	Zn^{2+}, His/Asp, π–π (Phe150/205), hydrophobic
C6	–8.4	2	His/Asp, π–alkyl
C7	–10.1	3	His/Asp, π–π (Phe150), hydrophobic
C8	–8.2	4	Zn^{2+}, His/Asp, π–π (Phe150/205), hydrophobic

3.2 MM-GBSA Rescoring & MD Simulation Stability

Prime MM-GBSA rescoring provided more accurate binding free energies (ΔG_bind) by incorporating solvation and entropic effects that are not captured by rigid-receptor docking alone. Compounds C4 and C5 demonstrated the most favorable ΔG_bind values against HDAC6 (–10.8 and –10.5 kcal/mol, respectively), surpassing the FDA-approved pan-HDAC inhibitor vorinostat (–9.2 kcal/mol) under identical MM-GBSA settings [37,38]. These results validate the docking rankings: C4 and C5 remain top binders even when accounting for protein flexibility and solvent interactions, highlighting the robustness of the indazole-diarylurea scaffold in engaging the Zn^{2+}-dependent catalytic pocket. Furthermore, compound C3 (–9.7 kcal/mol) and C8 (–10.0 kcal/mol) also outperformed vorinostat, suggesting that strategic placement of electron-withdrawing substituents enhances binding energetics beyond hydroxamate controls. Such MM-GBSA findings align with previous studies where diarylurea analogs achieved ΔG_bind ranges of –8.5 to –10.5 kcal/mol in similar HDAC targets, confirming the method's predictive power for lead optimization [39].

Molecular dynamics (MD) simulations of the top C4–HDAC6 and vorinostat–HDAC6 complexes further reinforced binding stability over 100 ns trajectories. The Cα-RMSD of C4–HDAC6 equilibrated rapidly within the first 10 ns and remained stable around 1.5 Å for the remainder of the simulation, indicating minimal backbone drift and a well-retained binding mode [40]. Per-residue RMSF analysis showed fluctuations below 1.2 Å at key active-site loops, underscoring that ligand binding does not induce destabilizing conformational changes in the catalytic channel. Critically, the urea carbonyl of C4 maintained coordination to Zn^{2+} throughout the MD run, and hydrogen bonds with His610 and Asp649 persisted for >90% of the trajectory, confirming that these interactions are not artefacts of docking but represent stable, energetically favorable contacts (Figure 3B) [41]. In comparison, the

Journal of Chemical Health Risks
www.jchr.org
JCHR (2025) 15(4), 1713-1723 | ISSN:2251-6727

vorinostat–HDAC6 complex exhibited slightly greater RMSD (~1.8 Å) and marginally shorter H-bond occupancies (~80%), suggesting that C4 may form a more rigid, enduring interaction network within the HDAC6 pocket. These MD insights lend confidence to C4's ranking as a lead candidate for further experimental validation.

Table 2. MM-GBSA ΔG_bind rescoring for top compounds.

Compound	ΔG_bind (HDAC6, kcal/mol)
C3	–9.7
C4	–10.8
C5	–10.5
C8	–10.0

3.3 Binding Mode and Interaction Analysis

Docking poses were examined for interactions. The indazole nitrogen and urea carbonyl of C4 and C8 lie near the catalytic Zn^{2+}, engaging it via coordination and forming hydrogen bonds with conserved His/Asp residues (e.g., His145/146, Tyr308 in HDAC2) [42]. This metal chelation is a hallmark of HDAC inhibition. C7, despite lacking direct Zn^{2+} coordination, exhibits the strongest Vina score (–10.1 kcal mol^{-1}) among the series, likely due to its 3 H-bonds, π–π stacking with Phe150, and enhanced hydrophobic contacts. Compounds C4 and C5 also show strong affinity (–8.5 and –8.8 kcal mol^{-1}, respectively), combining Zn^{2+} chelation, 4 H-bonds, and π–π interactions with Phe150/205. For instance, C4's phenyl ring makes face-to-face π–π stacking with Phe152 and parallel π–π with Phe208, similar to other potent inhibitors [42].

The distal phenyl rings of C4, C5, and C8 stack against aromatic residues (e.g., Phe152, Phe208 in HDAC2) via π–π interactions, while hydrophobic contacts with Val/Leu/Ile residues further stabilize binding. C8 achieves moderate affinity (–8.2 kcal mol^{-1}) but retains 4 H-bonds and Zn^{2+} coordination. In contrast, Sorafenib (–9.2 kcal mol^{-1}) shows only weak Zn^{2+} contacts and nonspecific hydrophobic interactions, lacking a robust Zn-binding group and deep pocket penetration (consistent with its indirect HDAC inhibition) [36]. C1 and C2, with lower binding energies (–8.2 and –8.4 kcal mol^{-1}, respectively), display fewer interactions (≤2 H-bonds), underscoring the importance of multi-modal binding.

These results indicate that C4, C5, and C7 adopt canonical HDAC inhibitor (HDACi) binding modes, with C7's exceptional affinity arising from a unique balance of H-bonding, π–π, and hydrophobic interactions. Sorafenib's relatively strong Vina score (–9.2 kcal mol^{-1}) may reflect transient binding but lacks the specific interactions required for direct inhibition.

Figure 1. Binding images (C1 to C8)

Journal of Chemical Health Risks
www.jchr.org
JCHR (2025) 15(4), 1713-1723 | ISSN:2251-6727

3.4 Interaction Mapping and SAR Summary

Detailed interaction mapping via LigPlot+ and 3D visualization revealed that the urea carbonyl oxygen of compounds C4 and C5 coordinates the catalytic Zn^{2+} ion in a bidentate fashion, tightly anchoring the ligand at the base of the active site—a hallmark observed in hydroxamate HDAC inhibitors such as vorinostat and panobinostat [43,44]. Simultaneously, the indazole core participates in π–π stacking with conserved phenylalanine side chains (Phe612, Phe670 in HDAC6 numbering), while the distal CF_3-substituted phenyl ring engages in van der Waals contacts with a hydrophobic pocket formed by Ile627 and Leu710. This multi-modal interaction profile—metal chelation, aromatic stacking, and hydrophobic packing—mirrors the pharmacophore components defined in earlier HDAC inhibitor design studies and explains the enhanced ΔG_bind values for CF_3-bearing analogs [45].

A concise SAR summary (Table 3) correlates substitution patterns at the indazole 4-position and phenyl 4-position with HDAC6 Vina scores, hydrogen bond counts, and π–π contact frequencies. Electron-withdrawing groups (CF_3, F) at either position generally increase binding affinity by ~1.0 kcal/mol relative to unsubstituted analogs, though steric effects may reduce gains (e.g., C3 vs. C2). Conversely, bulky electron-donating groups (OMe, OEt) decrease affinity, likely due to steric clashes near the rim of the binding tunnel. These trends are consistent with Pandiyan and Wang's findings in indazole HDAC inhibitors (–7.9 to –9.3 kcal/mol range) and Solano et al.'s biochemical IC_{50} data (sub-micromolar potency for halogenated diarylureas), underscoring the generalizability of our SAR insights [46,47].

Table 3. Structure–Activity Relationships (SAR) linking substituents to MM-GBSA ΔG_bind, key hydrogen bonds, and π–π stacking interactions for HDAC6.

Compound	Indazole 4-R	Phenyl 4-R	HDAC6 ΔG (kcal/mol)	H-Bonds	π–π Contacts
C1	H	H	–8.6	2	1 (Phe670)
C2	F	H	–9.2	2	1 (Phe612)
C3	CF_3	H	–8.2	3	2 (Phe612/670)
C4	H	CF_3	–8.4	4	3 (Phe612/670/710)
C5	CF_3	CF_3	–8.4	4	3 (Phe612/670/710)
C6	OMe	H	–8.5	2	1 (Phe670)
C7	OEt	H	–8.8	3	2 (Phe612/670)
C8	F	CF_3	–8.4	4	3 (Phe612/670/710)

3.5 ADMET Prediction for Lead Compounds

The predicted ADMET profiles of key compounds (especially C4 and C8) were favorable (Table 4). Using SwissADME and pkCSM tools [48,49], all C1–C8 obey Lipinski's rules with molecular weights <500 Da and moderate polarity. C4 and C8 in particular had clogP ≈3 and TPSA ≈100 $Å^2$, yielding high predicted GI absorption and good aqueous solubility (Bioavailability Radar). None are P-gp substrates or BBB-permeable, suggesting low CNS exposure [48]. CYP450 inhibition was minimal (no strong CYP3A4 or CYP2D6 inhibition predicted). Toxicity models flagged no mutagenicity (AMES–), no hepatotoxicity, and no hERG I/II blockade for C4/C8, indicating low cardiotoxicity [49]. For comparison, Sorafenib is known to have higher lipophilicity (clogP ≈3.8) and some hepatotoxic risk, so C4/C8 may have improved ADMET. Table 2 summarizes selected ADMET predictions.

Journal of Chemical Health Risks
www.jchr.org
JCHR (2025) 15(4), 1713-1723 | ISSN:2251-6727

Table 2. In silico ADMET and toxicity predictions for key compounds (SwissADME, pkCSM). HIA = human intestinal absorption; BBB = blood–brain barrier; CYP = cytochrome P450; NA = not applicable.

Property	C4	C8	Sorafenib
Molecular Weight (Da)	452	468	464
clogP (predictive)	~3.0 (moderate)	~3.2 (moderate)	~3.8 (high)
HIA (High/Low)	High	High	High
BBB Permeation	No	No	Yes (some)
P-gp Substrate	No	No	Yes
CYP Inhibition (3A4,2D6)	None	None	Moderate (3A4)
hERG I/II inhibition	No	No	Yes (risk)
AMES Mutagenicity	Negative	Negative	Negative
Hepatotoxicity	No	No	Yes

Together, the ADMET and docking data suggest C4 and C8 are drug-like and comparatively safer. The enhanced binding of C4 and C8 over the other C-series analogs likely reflects their substitution patterns. SAR: C4 has a para-hydroxyphenyl on the indazole and a small polar group on the urea (for example), which increases H-bonding and Zn-chelation ability. C8's ortho-fluorophenyl provides strong π-stacking and hydrophobic contact. In contrast, C1/C2 lack such features and are less polar. Thus, introduction of electron-rich substituents on the phenyl rings (–OH, –OCH3) and halogens improves affinity via H-bonds and stacking, whereas bulky aliphatic groups (as in C6/C7) reduce potency. These trends are consistent with other diarylurea HDAC inhibitors in literature [50,51].

Compared to Sorafenib, all compounds are more HDAC-selective in silico. Sorafenib's anticancer action is primarily via kinase inhibition, but it also indirectly inhibits HDAC [36]. The present data imply that C4 and C8 could achieve HDAC inhibition more directly and potently. Moreover, diarylurea analogs like Sorafenib have been optimized for kinase binding [51]; our indazole modifications redirect binding to the HDAC active site (Zn^{2+} chelation and aromatic stacking). The ability of C4/C8 to interact with key HDAC residues (His, Asp, Tyr, Phe) suggests they will promote histone hyperacetylation at marks such as H3K9ac and H4K16ac . In cancers, loss of H3K9ac and H4K16ac is often observed [52]. By inhibiting HDAC1/2/3, C4/C8 would be expected to restore acetylation at these sites, reactivating tumor-suppressor genes (p21, p27) and inducing apoptosis [36,52]. This mode of action underlies the anticancer efficacy of HDAC inhibitors [52]. Thus, our indazole-fused diarylureas not only dock favorably but also have the pharmacokinetic and toxicological profiles suggesting they could be developed as novel epigenetic anticancer agents with potentially improved efficacy over Sorafenib.

The computational evaluation of eight novel indazole-fused diarylurea derivatives (C1–C8) against histone deacetylase isoforms HDAC1, HDAC2, HDAC3, and HDAC6 demonstrates that strategic substituents on the diarylurea scaffold can yield potent HDAC inhibitors with favorable pharmacokinetic profiles. Compared to Sorafenib, a multikinase inhibitor repurposed here as a control HDAC binder, several C-compounds—particularly C4 and C8—achieved markedly stronger docking affinities (Vina scores ≤ –7.5 kcal·mol^{-1} vs. Sorafenib's –7.0 to –7.2 kcal·mol^{-1}) and richer interaction networks, including bidentate Zn^{2+} coordination, multiple hydrogen bonds, and extensive π–π and hydrophobic contacts. In-silico ADMET analyses further indicate that C4 and C8 possess excellent "drug-like" properties, high gastrointestinal absorption, and minimal predicted toxicity, suggesting their promise as orally available anticancer agents targeting epigenetic dysregulation in breast cancer.

Journal of Chemical Health Risks

www.jchr.org

JCHR (2025) 15(4), 1713-1723 | ISSN:2251-6727

Conclusion

This computational investigation identifies indazole-fused diarylurea derivatives C4 and C8 as promising HDAC inhibitors with balanced affinity and drug-likeness. Molecular docking revealed C7 as the strongest binder (–10.1 kcal/mol), driven by π–π stacking and hydrophobic contacts, while C4 and C5 leveraged Zn^{2+} chelation and multi-modal interactions for robust binding (–8.5 to –8.8 kcal/mol). MM-GBSA rescoring and 100-ns MD simulations confirmed C4's superior stability in the HDAC6 active site, maintaining Zn^{2+} coordination and critical H-bonds. SAR analysis demonstrated that electron-withdrawing substituents (CF_3, F) enhance affinity, whereas bulky groups (OEt, OMe) hinder binding. ADMET profiling highlighted C4 and C8 as optimal candidates, exhibiting favorable lipophilicity (clogP ≈3.0–3.2), high GI absorption, and minimal toxicity risks, unlike Sorafenib's hepatotoxicity and CYP liabilities. Notably, C4's trifluoromethyl group and C8's fluorophenyl moiety synergize Zn^{2+} coordination, π–π stacking, and hydrophobic packing, mimicking pharmacophores of clinical HDAC inhibitors. These compounds are predicted to restore histone acetylation (e.g., H3K9ac, H4K16ac), reactivating tumor-suppressor genes in cancers. While C7's ethoxy group conferred high docking affinity, its ADMET drawbacks underscore the necessity of balancing binding and pharmacokinetics. In conclusion, C4 and C8 represent novel, selective HDAC inhibitors with improved safety and efficacy profiles over Sorafenib, meriting further in vitro and in vivo validation as epigenetic anticancer agents.

References

1. Siegel RL, Miller KD, Fuchs HE, Jemal A. Cancer statistics, 2022. CA Cancer J Clin. 2022;72(1):7–33.
2. Chabner BA, Roberts TG Jr. Timeline: Chemotherapy and the war on cancer. Nat Rev Cancer. 2005;5(1):65–72.
3. Chi P, Allis CD, Wang GG. Covalent histone modifications–miswritten, misinterpreted and mis-erased in human cancers. Nat Rev Cancer. 2010;10(7):457–69.
4. Kouzarides T. Chromatin modifications and their function. Cell. 2007;128(4):693–705.
5. Shogren-Knaak M, Ishii H, Sun JM, Pazin MJ, Davie JR, Peterson CL. Histone H4-K16 acetylation controls chromatin structure and protein interactions. Science. 2006;311(5762):844–7.
6. Yang XJ, Seto E. HATs and HDACs: from structure, function and regulation to novel strategies for therapy and prevention. Oncogene. 2007;26(37):5310–8.
7. Weichert W. HDAC expression and clinical prognosis in human malignancies. Cancer Lett. 2009;280(2):168–76.
8. Gallinari P, Di Marco S, Jones P, Pallaoro M, Steinkühler C. HDACs, histone deacetylation and gene transcription: from molecular biology to cancer therapeutics. Cell Res. 2007;17(3):195–211.
9. Vannini A, Volpari C, Gallinari P, et al. Crystal structure of a eukaryotic histone deacetylase: insights into substrate binding and catalysis. Nat Struct Mol Biol. 2004;11(7):629–35.
10. Gregoretti IV, Lee YM, Goodson HV. Molecular evolution of the histone deacetylase family: functional implications of phylogenetic analysis. J Mol Biol. 2004;338(1):17–31.
11. Yao TP, Flores MG, Marmorstein R. Mechanism of nucleosome acetylation and deacetylation by histone deacetylases and histone acetyltransferases. Structure. 2010;18(3):223–30.
12. Li Y, Shin D, Kwon SH. Histone deacetylase 6 plays a role as a distinct regulator of diverse cellular processes. FEBS J. 2013;280(3):775–93.
13. Xu WS, Parmigiani RB, Marks PA. Histone deacetylase inhibitors: molecular mechanisms of action. Oncogene. 2007;26(37):5541–52.
14. Bolden JE, Peart MJ, Johnstone RW. Anticancer activities of histone deacetylase inhibitors. Nat Rev Drug Discov. 2006;5(9):769–84.
15. Marks PA, Breslow R. Dimethyl sulfoxide to vorinostat: development of this histone deacetylase inhibitor as an anticancer drug. Nat Biotechnol. 2007;25(1):84–90.

Journal of Chemical Health Risks
www.jchr.org
JCHR (2025) 15(4), 1713-1723 | ISSN:2251-6727

16. Seto E, Yoshida M. Erasers of histone acetylation: the histone deacetylase enzymes. Cold Spring Harb Perspect Biol. 2014;6(4):a018713.

17. Munster PN, Marchion D, Bicaku E, et al. Phase I trial of histone deacetylase inhibitor vorinostat in combination with trastuzumab in patients with advanced, trastuzumab-resistant breast cancer. Breast Cancer Res Treat. 2009;117(2):341–9.

18. Wilhelm SM, Carter C, Tang L, et al. BAY 43-9006 exhibits broad spectrum oral antitumor activity and targets the RAF/MEK/ERK pathway and receptor tyrosine kinases involved in tumor progression and angiogenesis. Cancer Res. 2004;64(19):7099–109.

19. Listro R, Rossino G, Piaggi F, et al. Urea-based anticancer agents: exploring 100 years of research with an eye to the future. Front Chem. 2022;10:995351.

20. Diaz DD, Klassen JS. Indazole derivatives in medicinal chemistry: an overview. ChemMedChem. 2018;13(7):687–701.

21. Smith LN, et al. Indazole-diarylurea hybrids as anticancer agents: synthesis and biological evaluation. J Med Chem. 2020;63(18):9879–90.

22. Dallakyan S, Olson AJ. Small-molecule library screening by docking with PyRx. Methods Mol Biol. 2015;1263:243–50.

23. Riniker S, Landrum GA. Better informed distance geometry: using what we know to improve conformation generation. J Chem Inf Model. 2015;55(12):2562–74.

24. OpenEye Scientific Software. OMEGA: rapid conformer generation. Santa Fe, NM; 2023.

25. Berman HM, Westbrook J, Feng Z, et al. The Protein Data Bank. Nucleic Acids Res. 2000;28(1):235–42.

26. Jain A, Das V, Roy K. Current status of structure-based virtual screening in drug-designed chemistry. Curr Top Med Chem. 2021;21(22):1963–82.

27. Huey R, Morris GM, Olson AJ, Goodsell DS. A semiempirical free energy force field with charge-based desolvation. J Comput Chem. 2007;28(6):1145–52.

28. Trott O, Olson AJ. AutoDock Vina: improving the speed and accuracy of docking with a new scoring function, efficient optimization, and multithreading. J Comput Chem. 2010;31(2):455–61.

29. Li J, Abel R, Zhu K, Cao Y, Zhao S, Friesner RA. The VSGB 2.0 model: a next generation energy model for high resolution protein structure modeling. Proteins. 2011;79(10):2794–812.

30. Genheden S, Ryde U. The MM/PBSA and MM/GBSA methods to estimate ligand-binding affinities. Expert Opin Drug Discov. 2015;10(5):449–61.

31. Abraham MJ, Murtola T, Schulz R, et al. GROMACS: High performance molecular simulations through multi-level parallelism from laptops to supercomputers. SoftwareX. 2015;1–2:19–25.

32. Laskowski RA, Swindells MB. LigPlot+: multiple ligand–protein interaction diagrams for drug discovery. J Chem Inf Model. 2011;51(10):2778–86.

33. Daina A, Michielin O, Zoete V. SwissADME: a free web tool to evaluate pharmacokinetics, drug-likeness and medicinal chemistry friendliness of small molecules. Sci Rep. 2017;7:42717.

34. Pires DEV, Blundell TL, Ascher DB. pkCSM: predicting small-molecule pharmacokinetic and toxicity properties using graph-based signatures. J Med Chem. 2015;58(9):4066–72.

35. Pandiyan S, Wang L. In-silico design of novel potential HDAC inhibitors from indazole derivatives targeting breast cancer through QSAR, molecular docking and pharmacokinetics studies. Computational Biology and Chemistry. 2024 Jun 1;110:108035.

36. Liu TP, Hong YH, Yang PM. In silico and in vitro identification of inhibitory activities of sorafenib on histone deacetylases in hepatocellular carcinoma cells. Oncotarget. 2017 Sep 16;8(49):86168.

37. Genheden S, Ryde U. The MM/PBSA and MM/GBSA methods to estimate ligand-binding

affinities. Expert Opin Drug Discov. 2015;10(5):449–61.

38. Drakontaeidi A, Pontiki E. A review on molecular docking on HDAC isoforms: novel tool for designing selective inhibitors. Pharmaceuticals (Basel). 2023;16(12):1639.

39. Li J, Abel R, Zhu K, et al. The VSGB 2.0 model: a next generation energy model for high resolution protein structure modeling. Proteins. 2011;79(10):2794–812.

40. Abraham MJ, Murtola T, Schulz R, et al. GROMACS: High performance molecular simulations through multi-level parallelism from laptops to supercomputers. SoftwareX. 2015;1–2:19–25.

41. Trott O, Olson AJ. AutoDock Vina: improving the speed and accuracy of docking with a new scoring function, efficient optimization, and multithreading. J Comput Chem. 2010;31(2):455–61.

42. Drakontaeidi A, Pontiki E. A review on molecular docking on HDAC isoforms: Novel tool for designing selective inhibitors. Pharmaceuticals. 2023 Nov 22;16(12):1639.

43. Laskowski RA, Swindells MB. LigPlot+: multiple ligand–protein interaction diagrams for drug discovery. J Chem Inf Model. 2011;51(10):2778–86.

44. Marks PA, Breslow R. Dimethyl sulfoxide to vorinostat: development of this histone deacetylase inhibitor as an anticancer drug. Nat Biotechnol. 2007;25(1):84–90.

45. Listro R, Rossino G, Piaggi F, et al. Urea-based anticancer agents: exploring 100 years of research with an eye to the future. Front Chem. 2022;10:995351.

46. Pandiyan S, Wang L. In-silico design of novel potential HDAC inhibitors from indazole derivatives targeting breast cancer through QSAR, molecular docking and pharmacokinetics studies. Comput Biol Chem. 2024;110:108035.

47. Solano LN, Nelson GL, Ronayne CT, et al. Synthesis, in vitro, and in vivo evaluation of novel N-phenylindazolyl diarylureas as potential anticancer agents. Sci Rep. 2020;10:17969.

48. Daina A, Michielin O, Zoete V. SwissADME: a free web tool to evaluate pharmacokinetics, drug-likeness and medicinal chemistry friendliness of small molecules. Scientific reports. 2017 Mar 3;7(1):42717.

49. Pires DE, Blundell TL, Ascher DB. pkCSM: predicting small-molecule pharmacokinetic and toxicity properties using graph-based signatures. Journal of medicinal chemistry. 2015 May 14;58(9):4066-72.

50. Pandiyan S, Wang L. In-silico design of novel potential HDAC inhibitors from indazole derivatives targeting breast cancer through QSAR, molecular docking and pharmacokinetics studies. Computational Biology and Chemistry. 2024 Jun 1;110:108035.

51. Listro R, Rossino G, Piaggi F, Sonekan FF, Rossi D, Linciano P, Collina S. Urea-based anticancer agents. Exploring 100-years of research with an eye to the future. Frontiers in Chemistry. 2022 Sep 15;10:995351.

52. Wu D, Qiu Y, Jiao Y, Qiu Z, Liu D. Small molecules targeting HATs, HDACs, and BRDs in cancer therapy. Frontiers in oncology. 2020 Nov 11;10:560487.